# Two-dimensional simulation of linear wave propagation in a suspension of polymeric microcapsules used as ultrasound contrast agents

Guillaume Haïat[a)]
*CNRS (Centre Nationale de la Recherche Scientifique), Université Paris-Est, Laboratoire Modélisation et Simulation Multi-Échelle, UMR (Unité mixte de recherche) 8208 CNRS, 94010 Créteil Cédex, France*

Romain Berti,[b)] Belfor Galaz,[b),c)] and Nicolas Taulier[b)]
*UPMC (Université Pierre et Marie Curie) Univ Paris 6, Laboratoire d'Imagerie Paramétrique, 15, rue de l'école de médecine, UMR 7623, 75006 Paris, France*

Jean-Jacques Amman
*Universidad de Santiago de Chile (USACH), Department of Physics, Ecuador 3493, Santiago, Chile*

Wladimir Urbach[b),d)]
*UPMC Univ Paris 6, Laboratoire d'Imagerie Paramétrique, 15, rue de l'école de médecine, UMR 7623, 75006 Paris, France*

(Received 18 June 2010; revised 16 December 2010; accepted 20 December 2010)

A generation of tissue-specific stable ultrasound contrast agent (UCA) composed of a polymeric capsule with a perfluorocarbone liquid core has become available. Despite promising uses in clinical practice, the acoustical behavior of such UCA suspensions remains unclear. A simulation code (2-D finite-difference time domain, FDTD) already validated for homogeneous particles [Galaz Haiat, Berti, Taulier, Amman and Urbach, (2010). J. Acoust. Soc. Am. **127**, 148–154] is used to model the ultrasound propagation in such UCA suspensions at 50 MHz to investigate the sensitivity of the ultrasonic parameters to physical parameters of UCA. The FDTD simulation code is validated by comparison with results obtained using a shell scatterer model. The attenuation coefficient (respectively, the sound velocity) increases (respectively, decreases) from 4.1 to 58.4 dB/cm (respectively, 1495 to 1428 m/s) when the concentration varies between 1.37 and 79.4 mg/ml, while the backscattered intensity increases non-linearly, showing that a concentration of around 30 mg/ml is sufficient to obtain optimal backscattering intensity. The acoustical parameters vary significantly as a function of the membrane thickness, longitudinal and transverse velocity, indicating that mode conversions in the membrane play an important role in the ultrasonic propagation. The results may be used to help manufacturers to conceive optimal liquid-filled UCA suspensions.
 [DOI: 10.1121/1.3543966]

PACS number(s): 43.80.Qf, 43.35.Bf, 43.20.Hq, 43.20.Px [CCC] Pages: 1642–1652

## I. INTRODUCTION

Recent advances in ultrasound imaging are due to the use of broadband transducers of increased bandwidth, resulting in higher axial resolution and allowing to shift to higher center ultrasonic frequencies. Higher lateral resolution is achieved, providing better images with higher contrast resolution. As in other imaging techniques, the use of ultrasound contrast agents (UCA) opens new diagnostic opportunities (Goldberg *et al*., 2001). These agents improve the image quality by increasing the backscattered echoes from the desired regions up to 25 dB, and the use of UCA may significantly improve high frequencies ultrasound imaging (Berson *et al*., 1999; Foster *et al*., 2000; Foster *et al*., 2002; Ketterling *et al*., 2007).

Recently, *in vivo* use of UCA at frequencies above 20 MHz has been suggested (Foster *et al*., 2000; Ketterling *et al*., 2007) for different applications involving microcirculation, ophthalmic disease diagnosis, and small animal imaging (Berson *et al*., 1999; Foster *et al*., 2002). The use of high frequency provides near-microscopic resolution for studies of development, atherosclerosis, tumor growth or angiogenesis, and drug effects (Goertz *et al*., 2002). At high frequency, the detection of second harmonic behavior of UCA may become difficult because of strong attenuation values. Consequently, new techniques are currently investigated, such as subharmonics imaging (Goertz *et al*., 2006; Cheung *et al*., 2008) and radial modulation imaging, (Cherin *et al*., 2008) and new UCA are specifically designed for high frequencies acoustic imaging. Investigations have been performed for instance at 40 MHz on lipid vesicles (Moran *et al*., 2006), at 50 MHz on polymer capsule with a perfluorocarbon liquid

[a)]Author to whom correspondence should be addressed. Electronic mail: guillaume.haiat@univ-paris-est.fr
[b)]Also at: CNRS, LIP, UMR 7623, 15, rue de l'école de médecine, 75006 Paris, France.
[c)]Also at: Universidad de Santiago de Chile (USACH), Department of Physics, Ecuador 3493, Santiago, Chile.
[d)]Also at: Laboratoire de Physique Statistique, École Normale Supérieure de Paris, CNRS UMR 8550, 24 rue Lhomond, 75005 Paris.

core (Pisani *et al.*, 2006), and in the range of 15 to 50 MHz on liquid perfluorocarbon emulsion (Couture *et al.*, 2006). Some of these new UCA have been functionalized to specifically target receptors (Diaz-Lopez *et al.*, 2009). In doing so, their concentration can be locally increased which in turn enhances the UCA response to ultrasound (Hughes *et al.*, 2005). It has also been shown that non-functionnalized UCA can aggregate or coalescence at a cancer tumor site (Rapoport *et al.*, 2007).

To pass through the lung capillaries and enter into the systemic circulation, microbubbles as a vascular contrast agent should be less than 10 $\mu$m in diameter (Keller *et al.*, 1987). Stability and persistence are the major concerns for such small microbubbles. Most vascular contrast agents are stabilized against dissolution and coalescence by the presence of additional materials such as polymeric proteins at the gas–liquid interface. In some cases, the material at the UCA outer interface is an elastic shell that enhances the microparticle stability. In other cases, the material is a lipid or a combination of two or more lipids. Moreover, newer agents use perfluorocarbon gases instead of air because of their low solubility in blood and high vapor pressure (Diaz-Lopez *et al.*, 2010). Thanks to this substitution, the stability and longevity of the agents have been markedly improved after intra-venous injection, usually lasting more than 5 min.

New clinical possibilities arise from tissue-specific ultrasound contrast agents, taken up by specific tissues, such as the reticuloendothelial system (Forsberg *et al.*, 1999). Some specific UCA may also adhere to specific sites such as venous thrombosis (Lanza *et al.*, 1996). These effects may require several minutes to several hours to reach maximum the effectiveness. For that reason, a new generation of stable contrast agents designed for therapeutic applications such as drug delivery or gene transfer has become available (Couture *et al.*, 2006; Pisani *et al.*, 2006). They are composed of a poly(lactic-co-glycolic acid) (PLGA) polymeric capsule with a liquid perfluorooctylbromide (PFOB) core.

Despite promising uses of UCA in clinical practice, the acoustical behavior of UCA suspensions still remains unclear, owing to the complexity of the involved modeling. This is unfortunate as the understanding of ultrasound propagation in UCA solutions is of great importance in the design and optimization of UCA for clinical use. To describe the interaction between a single isolated UCA particle and an ultrasonic wave, two different models based on (i) the Rayleigh-Plesset equation (Church, 1995; Allen *et al.*, 2002) and (ii) scattering phenomena have been derived in the literature. The Rayleigh-Plesset equation is based on dynamics of the motion of the bubble using the Navier-Stokes equations and is well adapted to the case of air-filled particle as large deformations of the particle radius may be taken into account. Scattering approaches are based on the computation of the scattering cross-section of each independent particle (de Jong *et al.*, 1992) and some of them allow the calculation of the acoustic radiation pressure on a coated particle (Hasegawa *et al.*, 1993). Such approaches assume low strain regime and the radius of the particle may only undergo variations of the first order. Scattering approaches are likely to be adapted to the case of liquid-filled particles treated herein because the fluid compressibility is much lower than that of gas, leading to lower deformation of the particle impacted by an ultrasonic wave. Moreover, discrepancies between measurements and predictions from single microbubble theories have been continuously observed, and multiple scattering phenomena have been evoked (Stride and Saffari, 2005) to explain these differences.

In a recent study by our group, a finite-difference time domain (FDTD) numerical simulation tool was applied to a suspension of elastic circular particles and validated around 50 MHz by comparison with an analytical model as well as experimentally (Galaz *et al.*, 2010). A potential advantage of a numerical approach is its ability to solve complex problems that may become rapidly intractable when following purely analytical approaches. Working in the time domain is interesting because (i) it allows a better comparison with the experimental signals which are obtained directly in the time domain and (ii) the ultrasonic velocities measured in the time domain using marker (such as the first zero crossing velocity) have been shown to be adapted for velocity measurements in a dispersive media such as bone (Haiat *et al.*, 2005; Haiat *et al.*, 2006). Another advantage of time domain numerical approaches over multiple scattering theories, which have been developed for both homogeneous (Waterman and Truell, 1961) and coated particles (Yang and Mal, 1994; Stride and Saffari, 2005), is that it allows simulating radio frequency (rf) signals directly in the time domain, avoiding reconstructions from the frequency domain (Insana *et al.*, 1990; Doyle, 2006). However, time domain numerical simulation tools have not been applied to model ultrasound propagation in UCA suspensions.

The aim of this study is to examine the problem of wave propagation at high frequency (50 MHz) in liquid-filled UCA suspensions using two-dimensional finite-difference time domain (2-D FDTD) numerical simulation tools. The main advantage of our numerical method is to deal with large population of UCA particles, allowing to simulate multiple scattering effects which have been shown to occur in such medium (Mobley *et al.*, 1999; Stride and Saffari, 2005; Chen and Zhu, 2006). We aim at estimating the physical determinants of the ultrasonic response of a UCA solution and the sensitivity of the ultrasonic parameters to the physical properties of the UCA suspension.

## II. MATERIALS AND METHODS

### A. Two-dimensional (2-D) numerical modeling

The method employed to perform the numerical simulation of wave propagation is similar to the one described in Galaz *et al.* (2010) and is briefly recalled in what follows. 2-D numerical simulations of ultrasonic wave propagation through identical randomly distributed microparticles solutions are performed using SIMSONIC, a FDTD simulation software developed by the Laboratoire d'Imagerie Paramétrique (Bossy *et al.*, 2004; Bossy *et al.*, 2005; Haiat *et al.*, 2007; Haiat *et al.*, 2008). Briefly, it uses an algorithm based on the spatial and temporal discretization of the two following first-order equations describing a 2-D linear elastic wave propagation (Bossy *et al.*, 2004).

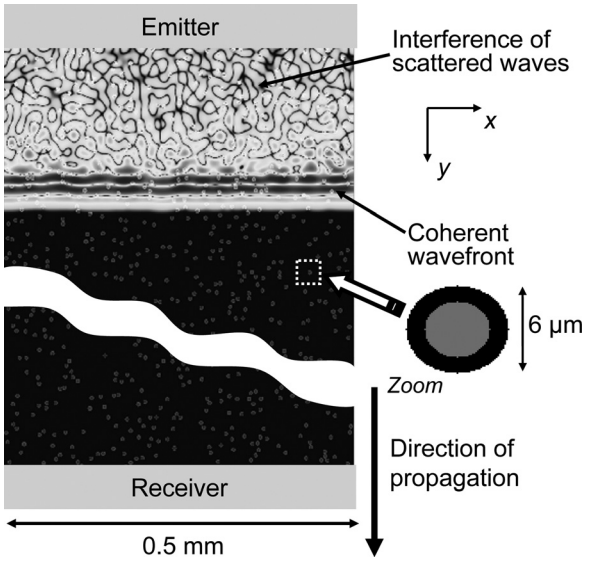


FIG. 1. Image illustrating the simulated propagation of ultrasonic wave in a suspension of ultrasound contrast agents. The curved separation represents an arbitrary split of the simulation domain. In the upper part of the figure, the gray scale codes the amplitude of the displacement as a function of position at a given time. In the lower part, the figure displays the random distribution of the particles. On the right hand side, an isolated particle is shown where black and gray pixels correspond, respectively, to elastic PLGA and liquid PFOB.

The main assumptions of the model are (i) all absorption phenomena are neglected, (ii) all heat transfer phenomena are neglected, and (iii) the temperature field is assumed to be constant and homogeneous. However, the model fully takes into account all reflection and refraction effects as well as mode conversions.

### B. Simulation domain

The simulation domain employed herein is similar to that used in (Galaz *et al.*, 2010). Briefly, the ultrasonic propagation is simulated in a $0.5 \times 1$ mm rectangular domain, as shown in Fig. 1. A linear ultrasound pressure source of 0.5 mm length located at $y = 0$ emits a broadband pressure pulse shown in black color in Fig. 2(a), with a center frequency equal to 50 MHz. Symmetric boundary conditions are applied to the box sides located at $x = 0$ and 0.5 mm. In order to avoid unphysical reflections due to the boundaries of the simulation mesh, perfectly matched layers (Collino and Tsogka, 2001) are positioned at $y = 0$ and 1 mm.

Two linear receivers located at $y = 0$ and 1 mm provide both backscattered and transmitted signals through a spatial average of the displacement over the entire transducers width (i.e., 0.5 mm). The chosen pixel size is equal to 0.1 $\mu$m, which is a compromise between an acceptable spatial resolution and a reasonable computational time (see Sec. III A for details).

An iterative probabilistic procedure described in details in Galaz *et al.* (2010) was used to randomly insert $N$ identical particles in the two-dimensional blank domain. We use this procedure to insert identical UCA particles composed of an inner circular region of radius, $P$, surrounded by a capsule whose thickness is denoted as $T$. The external radius $R$ of all particles is identical and equal to 3 $\mu$m, so that $P + T = R = 3$ $\mu$m. The right part of Fig. 1 shows the inserted UCA particle obtained by this procedure, where white zones correspond to water, black zones to PLGA capsule, and gray zones to PFOB core. Figure 1 also shows an image corresponding to the ultrasonic propagation in this heterogeneous medium where the gray scale codes the amplitude of the displacement as a function of space.

FDTD simulations require as input parameters mass densities and stiffness coefficients of all materials used in the simulation. The mechanical behavior of water and of POFB is that of liquid. PLGA is considered to have an isotropic elastic behavior. All mechanical properties of each material are summarized in Table I. The densities of PFOB and PLGA have been measured using a densimeter (model DMA 58, Anton Paar, Austria) and are in agreement with the literature (Andriano *et al.*, 1999; Karau *et al.*, 2001). The sound velocity in PFOB and the longitudinal velocity in PLGA were measured by classical time of flight techniques. Data concerning the Poisson's ratio and the transverse wave velocity in PLGA could not be found in the literature. As a first estimation, we choose a Poisson's ratio equal to 0.4, which is a typical value for most polymers (Powers and Caddell, 1972) and used this value to derive the transverse wave velocity of PLGA. These estimated values for PLGA material properties will be referred hereafter as "reference" material properties. Later, these material properties will be varied to explore their influence on ultrasound properties of UCA solutions.

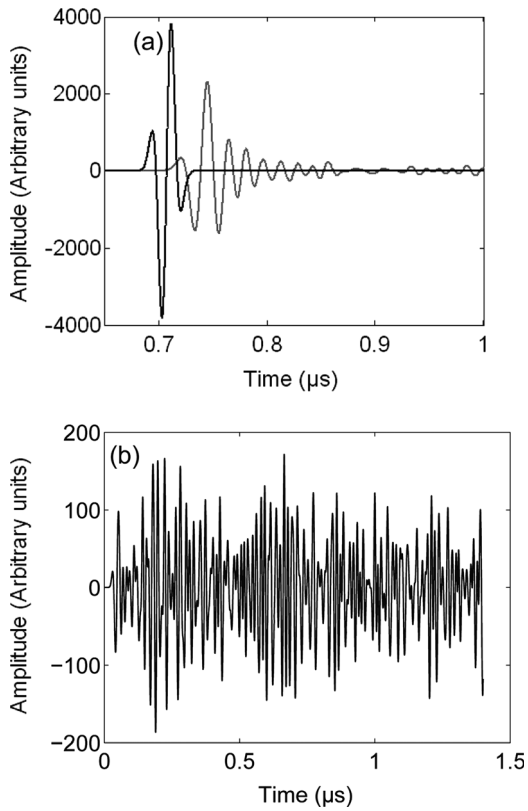


FIG. 2. Typical simulated rf signals. (a) The signal in water (in black) is identical in shape to the signal generated by the emitter. In gray, the rf signal transmitted in an ultrasound contrast agent solution. The particle concentration is $C = 60.41$ mg/ml. Each particle is surrounded by a $\mathrm{PLGA_R}$ capsule (see Table I). The capsule thickness tomicrosphere radius ratio $T/R = 0.35$. The value of the corresponding velocity (respectively, attenuation coefficient at 50 MHz) is equal to 1440 m/s (respectively, 45.1 dB/cm). (b) Backscattered rf signal obtained with the same UCA solution. The corresponding value of the relative backscattering intensity is equal to −18.4 dB/cm.

TABLE I. Density, stiffness coefficients and corresponding wave longitudinal and transverse propagation velocities ($V_L$ and $V_T$) of the different materials of interest. For PLGA, the first line corresponds to the reference properties (see text for details).

| | Material properties | | | Sound velocity | |
|---|---|---|---|---|---|
| | $\rho$ (g/ml) | $C_{11}$ (GPa) | $C_{55}$ (GPa) | $V_L$ (m/s) | $V_T$ (m/s) |
| Water | 1 | 2.25 | — | 1500 | — |
| PFOB | 1.935 | 1.0884 | — | 750 | — |
| $PLGA_R$ (reference) | 1.35 | 4 | 0.664 | 1721 | 701 |
| $PLGA_L$ (10% change in $V_{L,PLGA}$) | 1.35 | 4.84 | 0.664 | 1893 | 701 |
| $PLGA_T$ (10% change in $V_{T,PLGA}$) | 1.35 | 4 | 0.806 | 1721 | 773 |

### C. Comparison between numerical approach and experiments

In order to compare 2-D simulations with three-dimensional (3-D) experiments, a 2-D concentration equivalent to the experimental one needed to be determined. Similarly as what was done in Galaz *et al.*, (2010), we chose a method based on the mean distance between a particle and its closest neighbor since it is a meaningful parameter in two and three dimensions. For $N$ randomly distributed particles within an sufficiently large 2-D domain of surface area $S$, the particle concentration writes (Galaz *et al.*, 2010)

$$C = M\left(\frac{N}{S}\right)^{3/2}, \tag{1}$$

where $M$ is the mass of a particle.

### D. Determination of the ultrasonic parameters

Basic signal processing techniques were applied to the simulated rf signals to retrieve the ultrasound properties of the 2-D domain. An example of simulated rf signal obtained in transmission and in backscattering is shown in Figs. 2(a) and 2(b), respectively. Three parameters extracted from the simulations and experimental measurements were the speed of sound, $V$, the attenuation coefficient, $\alpha(f)$, and the relative backscattered intensity $I_B$. Since absorption is neglected in the simulations, the attenuation obtained *in silico* is only due to the scattering phenomena and the corresponding $\alpha(f)$ value, in decibels, is given by (D'Astous and Foster, 1986)

$$\alpha(f) = \frac{10}{L}\log\left(\frac{S_{\mathrm{ref}}(f)}{S_{\mathrm{Sol}}(f)}\right), \tag{2}$$

where $L$ is the path length of sound propagation (here, $L=1$ mm). $S_{\mathrm{ref}}(f)$ and $S_{\mathrm{sol}}(f)$ are, respectively, the power spectrum densities (PSDs) of the signal transmitted in water and in the solution, obtained using a fast Fourier transform. The apparent backscattered coefficient, ABC($f$), expressed in decibels, is given by (Chaffai *et al.*, 2000)

$$\mathrm{ABC}(f) = 10\log\left(\frac{S_b(f)}{S_{\mathrm{ref}}(f)}\right), \tag{3}$$

where $Sb(f)$ is the PSD of the backscattered signal recorded by the transducer located at $y=0$. The relative backscattered intensity $I_B$ (which does not depend on the frequency) is then computed by averaging the ABC($f$), over the frequency bandwidth of interest (35–62 MHz).

## III. RESULTS AND DISCUSSION

### A. Analytical validation

In order to validate our numerical approach in the framework of UCA suspensions, simulations in a 2-D domain containing a single microparticle (described in Sec. II B) made of a PLGA shell surrounding liquid PFOB have been carried out. The inner circular region of this single particle has a radius $P=1.95$ $\mu$m and its shell thickness is equal to 1.05 $\mu$m ($T/R=0.35$). This kind of system (disk-shaped shell model) has been analytically solved (Goodman and Stern, 1962; Doolittle and Uberall, 1966; Ugincius and Uberall, 1968; Hasegawa *et al.*, 1993) for any angle of observation and of incidence when an isolated coated particle is considered. The reader is referred to these publications for further details on the analytical model. Figure 3 shows the comparison between the angular scattering cross-section (at 180° and 90°) obtained (i) with the analytical model applied to a lossless isotropic elastic cylinder immersed in water and (ii) by computing the amplitude ratio of the FDTD

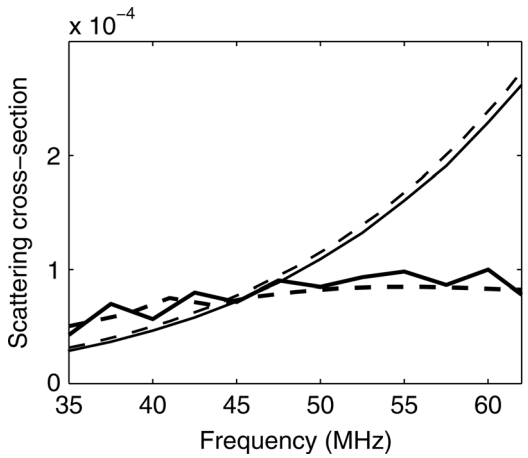


FIG. 3. Scattering cross-section obtained with the shell model (dashed lines) and the numerical simulation (solid lines) at angles of 180° (thick lines) and 90° (thin lines) from the incident beam.

numerically simulated spectra of the scattered signal to the incident signal. A fair agreement is obtained between both approaches. We verified that the total surface of the particle is conserved by the numerical model as it is equal to $28.27 \times 10^{-12}$ m$^2$ for the analytical model (real disk) and to $28.21 \times 10^{-12}$ m$^2$ for the numerical approach (meshed disk). Therefore, the slight discrepancy between the analytical and numerical results, which is always lower than 15%, is not likely to come from a difference in particle size and could be rather due to the (constant) spatial discretization (0.1 $\mu$m) used in the simulation code, as shown in Fig. 1. We have checked (data not shown) that increasing the discretization step in the numerical model leads to an increase in the discrepancy between the analytical and numerical model. However, decreasing the mesh size below 100 nm could lead to possible problems since we are tackling the limit of continuum mechanics. Moreover, decreasing the spatial discretization would lead to significantly higher computation time. The spatial discretization equal to 100 nm corresponds to a compromise between continuum mechanics regime, computation time, and reasonable accuracy of the computations.

The total scattering cross-section $\gamma_{sca}$ can be obtained for one particle using the shell scattering model (which does not assume that the situation is in the Rayleigh domain) by integrating the angular scattering cross-section around the particle. Figure 4 shows the variation of $\gamma_{sca}$ as a function of frequency between 0 and 100 MHz. The results shown in Fig. 4 indicate (data not shown) that the total scattering cross-section varies approximately as $f^{3.4}$ in the bandwidth of interest. The frequency dependence of the scattering cross-section is different from that of Rayleigh scattering ($f^4$ would be obtained) because the ratio of the wavelength and of the diameter is approximately equal to 5, which is not in the scope of the Rayleigh approximation. Moreover, a resonance phenomenon is shown to occur around 77 MHz, which is out of the frequency bandwidth of interest.

Since the simulation code predicts reasonably well the ultrasonic properties of a single particle, our investigation was extended (i) to study the influence of the membrane properties (material properties and membrane thickness) on the total scattering cross-section using the analytical model and (ii) to the case of a distribution of similar particles. For this case, to the best of our knowledge, there is no analytical model available in the time domain.

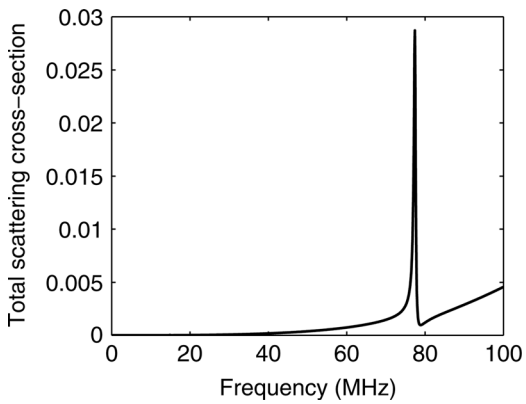


FIG. 4. Variation of the total scattering cross-section $\gamma_{sca}$ as a function of frequency between 0 and 100 MHz predicted by the shell scattering model. A resonance is obtained around 77 MHz.

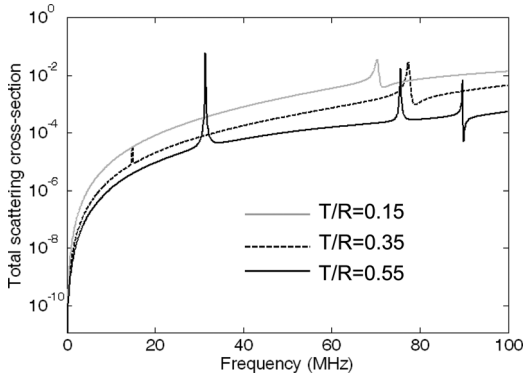


FIG. 5. Total scattering cross-section predicted by the shell model for different values of membrane thicknesses. The results are given in logarithmic scale.

## B. Scattering response of an isolated particle

In order to better understand the results with a population of particle, we have conducted simulations where the scattering cross-section of a single particle is studied as a function of the shell properties (elastic constants, mass density, and membrane thickness), which allows to interpret the variation in the scattering properties of a population of particles. Figure 5 shows the variation of the total scattering cross-section as a function of frequency of different values of $T/R$ equal to 0.15, 0.35, and 0.55. As shown in Fig. 5, increasing the value of $T/R$ leads to an increase of the scattering cross-section in the frequency bandwidth of interest as well as to an increase of the values of the resonance frequency. In the case of $T/R = 0.55$, additional resonance frequencies can also be noted.

Figure 6 shows the variation of the total scattering cross-section as a function of frequency for different values of the shell material properties indicated in Table I. The solid gray (respectively, gray) line corresponds to the reference

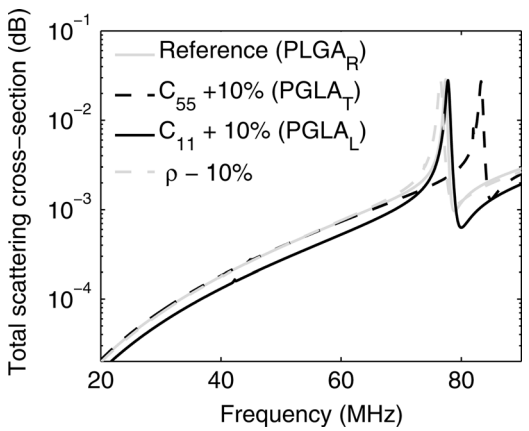


FIG. 6. Total scattering cross-section predicted by the shell model for different values of material properties. The results are given in logarithmic scale. The solid gray line corresponds to the reference material properties given in Table I. The solid black line corresponds to the material properties denoted the PLGA$_L$ in Table I. The dashed black line corresponds to the material properties denoted the PLGA$_T$ in Table I. The dashed gray line corresponds to the material reference material properties indicated in Table 1 with a value of PLGA mass density equal to 1.215 g/ml.

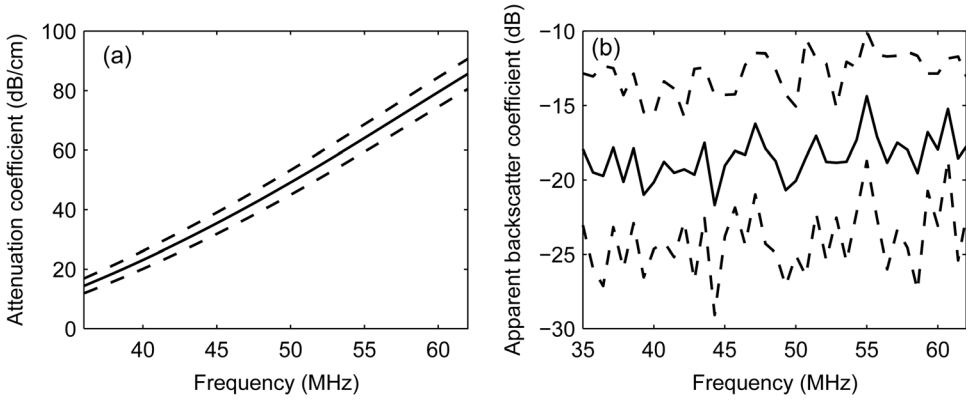


FIG. 7. (a) Mean attenuation coefficient and (b) apparent backscattering cross-section obtained when averaging the results obtained with 15 solutions with $C = 60.41$ mg/ml and $T/R = 0.35$. The two dashed lines in (a) and (b) represent the sum and the subtraction of the mean and of the standard deviation of each quantity.

material properties given in Table I (respectively, the material properties denoted $PLGA_L$ in Table I). The dashed black line corresponds to the material properties denoted as $PLGA_T$ in Table I. The dashed gray line corresponds to the material reference material properties indicated in Table I with a value of PLGA mass density equal to 1.215 g/ml. The results shown in Fig. 6 indicate that the total scattering cross-section weakly depends on the variations of $C_{55}$ and of mass density of the membrane within the frequency bandwidth of interest. However, an increase of $C_{11}$ in PLGA induces a decrease of the total scattering cross-section in the bandwidth of interest. The value of the resonance frequency (around 77 MHz for the reference material properties) depends on the values of $C_{55}$ in PLGA and (to a lesser extent) of mass density. However, $C_{11}$ weakly affects the value of the resonance frequency. Variations of the membrane material properties indicated in Table I have a weaker effect compared to that of variations of $T/R$ between 0.15 and 0.55. Therefore, the values of $T/R$ seem to be a parameter of importance relatively to the ultrasonic response of the particle.

### C. Ultrasound contrast agent solutions

The ultrasonic properties (ultrasonic velocity, attenuation, and relative backscattered intensity) of a given solution constructed using the procedure described in Sec. II B depend on the realization of the random distribution of UCA particles and the ultrasonic parameters may differ for two solutions constructed using the same parameters. For each set of parameters (concentration, particle geometry, density, and longitudinal and transverse speeds of sound of the membrane) considered in what follows, 15 different solutions corresponding to 15 cases with a different random placement of particles were considered and the ultrasonic parameters were averaged over the 15 solutions. This value (15) corresponds to a compromise between reasonable computation time and an acceptable convergence of the ultrasonic parameters. An increase in the number of simulated solutions from 15 to 25 induces a relative change of the averaged attenuation coefficient equal to 4%, of the averaged $I_B$ of 2% and no change of the averaged velocity. These values are significantly lower than the standard deviation of the results, which corresponds to the variation due to the random spatial distribution of the particles in the simulation domain.

Figure 2(a) shows simulated signals transmitted through water and through the solution of UCA particles both recorded at $y = 1$ mm. The corresponding backscattered signal recorded at $y = 0$ mm is shown in Fig. 2(b).

Figure 7(a) shows the variation of the attenuation coefficient between 35 and 62 MHz, averaged for 15 different solution constructed using the same parameters ($T/R = 0.35$, $C = 60.41$ mg/ml). A concentration equal to 60.41 mg/ml has been chosen because this value corresponds to the highest concentration used in the experimental work of Pisani *et al.* (2008). The two dashed lines represent the sum and the subtraction of the mean and of the standard deviation values of the attenuation coefficient. A plot in logarithmic coordinates of the averaged attenuation coefficient indicates (data not shown) that the attenuation coefficient varies approximately proportionally to $f^{3.2}$ in the bandwidth of interest. If independent scattering is assumed in the solution, the attenuation coefficient is proportional to the total scattering cross-section $\gamma_{sca}$ obtained for one particle (Biwa *et al.*, 2003). Assuming independent scattering and using the shell scattering model described in Sec. III A lead to a frequency dependent attenuation coefficient obtained analytically varying as $f^{3.4,}$ which is in the same order of magnitude than the frequency dependence of the attenuation coefficient obtained numerically. The difference between the two results may come from the influence of multiple scattering phenomena.

The corresponding variation of the ABC($f$) is represented with a solid line in Fig. 7(b). Again, the two dashed lines indicate the sum and the subtraction of the mean and of the standard deviation values of ABC($f$). The ABC is shown to weakly depend on frequency, which may be explained by analyzing the angular scattering cross-section at 180° obtained analytically for one particle (thick lines of Fig. 3), which also exhibits a weak frequency dependence.

#### 1. Effect of concentration

When dealing with UCA, it is important to know the concentration of particles that should be injected to produce the optimum effect. For this reason, we have investigated the effect of concentration on the speed of sound, attenuation, and backscattered intensity. Eight concentrations, ranging

TABLE II. Number $N$ of particles accounted for in the simulation domain, of the corresponding ultrasound contrast agent concentration, of the particle volume fraction and of the mean inter-particule distance ($D_2$).

| $N$ | 80 | 150 | 250 | 400 | 600 | 800 | 1000 | 1200 |
|---|---|---|---|---|---|---|---|---|
| $C$ (mg/ml) | 1.37 | 3.51 | 7.55 | 15.28 | 28.07 | 43.22 | 60.41 | 79.4 |
| Particle volume fraction (%) | 1.1 | 2.1 | 3.5 | 5.6 | 8.5 | 11.3 | 14.1 | 16.9 |
| $D_2$ ($\mu$m) | 79 | 57.7 | 44.7 | 35.4 | 28.9 | 25 | 22.4 | 20.4 |

from 1.37 to 79.4 mg/ml, were used herein and are listed in Table II with the corresponding values of $N$ obtained from Eq. (1). This range of concentration corresponds to the concentration range that has been experimentally investigated by Pisani *et al*. (2008) for their ultrasound contrast agent. Since our simulations aim at investigating their results with the use of simulation, we obviously used the same concentration range as the authors. Note that the initial concentration of SonoVue (a commercially available ultrasound contrast agent, UCA) is about $1–5 \times 10^8$ microbubbles/ml (Schneider, 1999). After intra-venous injection, the SonoVue concentration decreases rapidly and SonoVue microbubbles have mostly disappeared after 11 min. The above 79.4 mg/ml correspond to a concentration of $5\times10^8$ nanoparticles/ml, which is the initial concentration of a regular preparation of commercial UCA. All the smaller concentrations investigated in this study reflect a progressive dilution of the preparation after injection.

Figure 8(a) shows that the attenuation coefficient at 50 MHz increases with the UCA concentration. Moreover, as shown in Fig. 8(b), the relative backscattered intensity $I_B$ also increases with the concentration and the saturation can be observed for high concentration values, which may be due to the multiple scattering phenomena. The simulated data of Fig. 8(b) are compared with the corresponding experimental results (indicated by triangles) published previously by our group (Pisani *et al*., 2008). In the experiments, the relative backscattered intensity is normalized by the electronic noise level, which is not possible in the simulations where no noise is present. Therefore, a modified backscattered intensity was defined in the simulation. We added 32 dB to the simulated relative backscattered intensity, so that the extrapolated value at zero concentration in microparticles falls down to zero. Therefore, the results shown in Fig. 8(b) only compare the variation of backscattered energy *versus* the concentration of particles and not its absolute value. Note that the different methods (O'Donnel and Miller, 1981; Roberjot *et al*., 1996; Chaffai *et al*., 2000) have been devised in order to correct backscatter measurements from the influence of attenuation. However, these methods were not implemented in this work, as our goal was not to retrieve the real backscatter coefficient of the solution but to assess ultrasonic parameter which can be easily measured experimentally.

The results shown in Figs. 8(a) and 8(b) may be analyzed in order to determine the concentration above which multiple scattering plays a role. When independent scattering is assumed, the attenuation coefficient and the ABC are proportional to the concentration (Biwa *et al*., 2003), which is

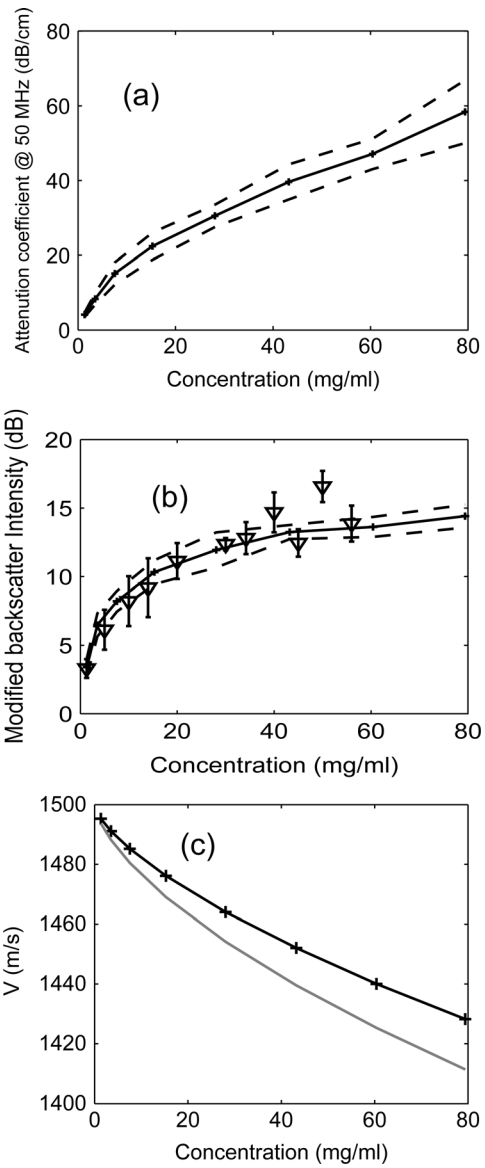


FIG. 8. (a) Mean attenuation coefficient at 50 MHz, (b) modified backscattered intensity $I_B$, and (c) speed of sound and as a function of UCA concentration for a ratio $T/R = 0.35$. The black solid lines correspond to numerical results. The two dashed lines in (a) and (b) represent the sum and the subtraction of the mean and of the standard deviation of each quantity. The gray line in (c) indicates the results obtained with a shell effective medium model. The triangles in (b) correspond to the corresponding experimental results published in Pisani *et al*. (2008).

not necessarily the case when multiple scattering occurs. Therefore, an empirical way to determine an order of magnitude of the concentration above which multiple scattering plays a role consists in assessing the concentration above which the attenuation and the ABC starts varying non-linearly. An analysis of Figs. 8(a) and 8(b) shows that multiple scattering is likely to occur above approximately 7 mg/ml. Moreover, above around 7 mg/ml, the wavelength in water (30 $\mu$m at 50 MHz) is of the same order of magnitude or lower than the mean inter particle distance (see Table II). This situation indicates that multiple scattering is likely to be significant, viscous absorption being neglected. However, the determination of such concentration remains empirical as

it may be difficult to estimate such value accurately (Haiat and Naili, 2011).

The black line in Fig. 8(c) shows that the sound velocity decreases as the concentration of UCA disks increases. The standard deviation for $V$ values is always lower than 1.3 m/s (data not shown). The gray line shows the results obtained for the variation of the sound velocity as a function of the concentration using the shell effective medium model used in Sec. III A. The numerical results are in qualitative agreement with the analytical results.

To conclude, our simulations show that UCA are the most efficient (i.e., exhibit the largest $I_b$ value) for concentration higher than 30 mg/ml, in good agreement with experimental data (Pisani *et al.*, 2008). Note that the small gain obtained using much higher concentration may not be worthy as large concentration of UCA may induce side effects in the organism.

### 2. Influence of capsule thickness

Most commercial UCA possess a very thin capsule thickness. This feature has been used in most theoretical models as it provides a useful approximation that greatly simplifies analytical approaches. The use of thick polymeric capsule becomes popular (Bjerknes *et al.*, 1997; Chen *et al.*, 2003; Pisani *et al.*, 2006) as it reduces the diffusion of the encapsulated perfluorocarbon fluid and increases the UCA stability. That is why we have investigated the influence of capsule thickness to the ultrasound properties of an UCA solution. Five different $T/R$ values were simulated for an identical number of particles ($N=1000$ and $D_2=22.4$ $\mu$m, which represents a distance seven times greater than the radius) and using the PLGA reference material properties. The values of $T/R$ (ratio of the membrane thickness over the particle radius) were chosen to approximately correspond to typical values which are likely to be achieved experimentally, that is $T/R=0.15$, 0.25, 0.35, 0.45, and 0.55. The corresponding values of the membrane thickness and of the concentration are shown in Table III.

Figure 9(a) shows that an increase in capsule thickness induces an important decrease in the attenuation coefficient at 50 MHz especially for low values of $T/R$**.** These results are consistent with previous results showing that the response of UCA solution is strongly influenced by the shell properties (Deng *et al.*, 1998; Postema and Schmitz, 2007).

The behavior of $I_B$ as a function of $T/R$ is more complex as shown in Fig. 9(b). For $T/R<0.35$, $I_B$ decreases as $T/R$ increases and reaches a minimum value for $T/R=0.35$. For low $T/R$ values (thin membrane), the decrease in $I_B$ is consistent with the decrease in attenuation obtained in the last paragraph. The strong attenuation obtained for low $T/R$ values implies that only the region located nearby the emitter contributes to the backscattered signal. However, for $T/R>0.35$, the size of the region contributing to the backscattered signal increases due to a decrease in attenuation, which may explain the observed increase in $I_B$. In summary, two competing phenomena contribute to $I_B$: the increase in the size of the insonified region and the decreasing attenuation.

As shown by the black line in Fig. 9(c), an increase in sound velocity is observed when $T/R$ increases, which is consistent with the result obtained with the shell effective medium model (Goodman and Stern, 1962; Doolittle and Uberall, 1966; Ugincius and Uberall, 1968; Hasegawa *et al.*, 1993) represented with a gray line in Fig. 9(c).

TABLE III. Values of the membrane thickness and of the concentration as a function of the $T/R$ values. Here, $R=3$ $\mu$m, the number of particle $N$ is equal to 1000 and $D_2=25$ $\mu$m.

| $T/R$ | 0.15 | 0.25 | 0.35 | 0.45 | 0.55 |
|---|---|---|---|---|---|
| Membrane thickness ($\mu$m) | 0.45 | 0.75 | 1.05 | 1.35 | 1.65 |
| $C$ (mg/ml) | 68.35 | 63.85 | 60.41 | 57.87 | 56.11 |

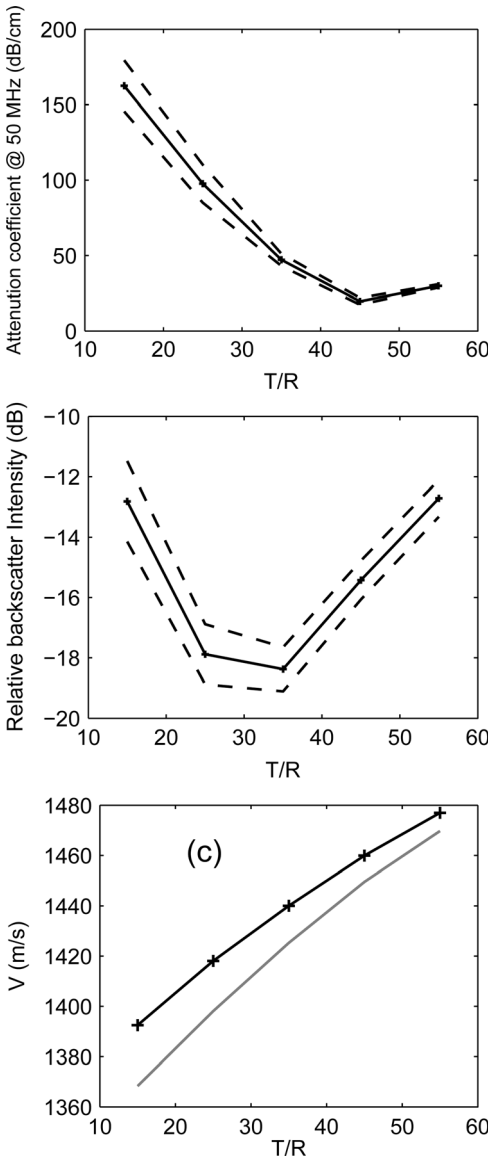


FIG. 9. (a) Mean attenuation coefficient at 50 MHz, (b) relative backscattered intensity $I_B$, and (c) speed of sound and as a function $T/R$ for UCA concentration $C=60.4$ mg/ml. The black solid lines correspond to numerical results. The two dashed lines in (a) and (b) represent the sum and the subtraction of the mean and of the standard deviation of each quantity. The gray line in (c) indicates the results obtained with the shell effective medium model.

TABLE IV. UCA solution ultrasonic properties at $C = 60.41$ mg/ml for different properties of PLGA capsule (see Table I).

| Type of PLGA capsule | $PLGA_R$ | $PLGA_L$ | $PLGA_T$ |
|---|---|---|---|
| Sound velocity in UCA solution (m/s) | 1440 ± 0.1 | 1450 ± 0.1 | 1442 ± 0.1 |
| Attenuation coefficient at 50 MHz (dB/cm) | 47.1 ± 3.1 | 38.5 ± 2.9 | 45.6 ± 4.5 |
| Relative backscattering intensity (dB) | −18.4 ± 0.8 | −15.1 ± 1.1 | −18.5 ± 0.9 |

#### 3. Effect of polymer properties

It has been shown that PLGA microspheres exhibit different mechanical properties depending on the ratio of lactic to glycolic acid used to produce the PLGA copolymer (Eliaz and Kost, 2000; Chung *et al.*, 2006). Since PLGA microparticles used in drug delivery or in UCA are usually made of an equal quantity of lactic and glycolic acids (i.e., 50/50 PLGA), we used their properties as a reference. To investigate possible effects of a change in the lactic to glycolic acid ratio and consequently of the capsule properties, we performed simulations for different PLGA properties at the same concentration ($C = 60.41$ mg/ml) and for an identical ratio ($T/R = 0.35$), as displayed in Table I. The first one corresponds to the reference material properties (of 50/50 PLGA) that were used for all our previous simulations. The second (respectively, third) one corresponds to the same transverse (respectively, longitudinal) wave velocity but with different longitudinal (transverse) wave velocity $V_{L,\mathrm{PLGA}}$ ($V_{T,\mathrm{PLGA}}$) increased of an amount of 10% as compared to the reference case (see Table IV). Both changes in $V_{L,\mathrm{PLGA}}$ and $V_{T,\mathrm{PLGA}}$ may be achieved by varying the ratio of lactic to glycolic acid.

The simulations show that the UCA efficiency is weakly influenced by changes in transverse velocity of the membrane ($V_{T,\mathrm{PLGA}}$) since the value of $I_B$ is nearly insensitive to the increase of 10% of the transverse sound speed in the polymer (see Table IV). However, the backscattering response increases significantly from −18.4 to −15.1 dB when the longitudinal velocity increases of 10%. The speed of sound in solution increases by 10 m/s when the longitudinal velocity increases by 10% and by 2 m/s for the same increase in the transverse velocity. As shown in Table IV, the attenuation coefficient at 50 MHz depends on changes in both $V_{T,\mathrm{PLGA}}$ and $V_{L,\mathrm{PLGA}}$, although this dependence is stronger when $V_{L,\mathrm{PLGA}}$ varies. These results are in agreement with the results obtained in Sec. III B 2, showing that the capsule properties have an important impact on the ultrasonic attenuation. The dependence of attenuation and of the velocity on changes of $V_{T,\mathrm{PLGA}}$ shows that the contribution of polymer properties to ultrasound parameters is not straightforward and suggest that mode conversions and transverse wave propagation in PLGA may play a significant role.

### D. Limitation of the study

Ultrasonic attenuation results from a combination of scattering and absorption phenomena. Absorption effects are not taken into account although viscous and viscoelastic effects (Hoff *et al.*, 2000; Sarkar *et al.*, 2005) have been shown to play a role in the ultrasonic propagation in UCA suspensions. The complete characterization of absorption requires the knowledge of a large number of thermo-physical parameters that are in practice hard to quantify. Only the part of attenuation that depends on scattering phenomena, particle concentration and structural properties, ultrasound wave frequency, and impedance mismatch between water and particles is considered here. The difference between the present study and Galaz *et al.* (2010) mainly lies in the geometry of the particles, which are now filled with liquid whereas they were homogeneous elastic solid in the previous study. Previously, we were able to obtain a reasonable agreement between numerical and experimental results without introducing any absorption phenomena. This agreement justifies the use of the same approximation in the present manuscript as introducing liquid in the particle adds an interface and could thus induce an increase of scattering phenomena relatively to absorption phenomena. However, neglecting absorption is a simplistic approximation and viscous absorption should be included in the future. The attenuation coefficient at 50 MHz in water is equal to 5.4 dB/cm (Krautkramer and Krautkramer, 1990), which corresponds approximately to the attenuation value predicted by our model for the lowest concentration tested herein ($C_0 = 1.37$ mg/ml). For concentration lower than $C_0$, viscous absorption in the surrounding fluid should therefore be a dominating phenomenon, whereas for concentration higher than $C_0$, viscous absorption in the surrounding fluid is expected to play a minor role in the propagation compared to that of scattering phenomena.

The SIMSONIC code does not take into account any nonlinear ultrasonic behavior, such as harmonic generation or radiation pressure (Sun *et al.*, 2005; Ketterling *et al.*, 2007), which cannot be modeled. This limitation is important because in the context of ultrasound contrast agents, non-linear effects are known to play an important role. However, while non-linear effects have been widely investigated for air-filled particles, it remains poorly understood for liquid-filled particles such as these investigated herein.

The present results can not be used in order to study the polymer shell agents produced by for instance Point Biomedical, Acusphere, or Bracco because these are air-filled particles and are therefore likely to behave in a different manner. This paper deals exclusively with liquid-filled agents developed by our group. Such particles behave quite differently than gas filled agents, which are more acoustically active than liquid-filled agents. For now, the FDTD model used herein is currently not able to model the interface between a solid and a gas.

We choose to consider monodisperse suspensions in order to study the effect of concentration independently of the diameter distribution, which corresponds to a first step in the study of such suspensions.

In the present study, the case of randomly spatially distributed particles is studied, which could also be tackled by analytical models in the frequency domain. However, the advantage of our approach is that it is suitable to model the acoustical response of non-uniformly distributed contrast

agents in a medium, like in the case of particles targeted on a specific tissue, attached to a vessel wall, whereas some other particles are randomly distributed in the rest of the lumen.

In this paper, we use a 2-D model although 3-D models would be more accurate to model the propagation in UCA suspensions, which is possible using the SIMSONIC Software (Bossy *et al.*, 2005; Haiat *et al.*, 2007). The propagation in a 2-D medium of disks is different than in a 3-D medium of spheres, which might explain possible discrepancies experiments and simulations. First, 3-D simulations will lead to a more realistic situation in terms of particle spatial distribution and volume fraction as the model described in Sec. II C would not be needed. In particular, in 3-D, a linear relationship will be obtained between the concentration and volume fraction, which is not the case herein. Second, the scattering cross-section of a cylinder and of a sphere is different, which may also significantly modify the results. 3-D simulations should be carried out in the future in order to give further insight on such differences. The present 2-D approach is a first step in studying these phenomena and further studies are required to tackle the difficult 3-D problem, which would require significantly longer time of computation and memory in the framework of UCA.

Despite the limitations stated above, our FDTD numerical simulation tool proves to be a promising approach to better understand the physical determinants that influences ultrasound propagation in UCA suspensions. It should help UCA manufacturers to design more efficient particles by relating the physical properties of the UCA solution with the expected ultrasound response. The next logical step will be to turn toward 3-D simulations.

## ACKNOWLEDGMENTS

The authors B.G., R.B., N.T., and W.U. acknowledge the financial support from ANR (Agence Nationale de la Recherche, ACUVA n° NT05-3_42548) and from EC-FP6-project DiMI, LSHB-CT-2005-512146.

Allen, J. S. III, May, D. J., and Ferrara, K. W. (**2002**). "Dynamics of therapeutic ultrasound contrast agents," Ultrasound Med. Biol. **28**, 805–816.

Andriano, K. P., Tabata, Y., Ikada, Y., and Heller, J. (**1999**). "*In vitro* and *in vivo* comparison of bulk and surface hydrolysis in absorbable polymer scaffolds for tissue engineering," J. Biomed. Mater. Res. **48**, 602–612.

Berson, M., Gregoire, J. M., Gens, F., Rateau, J., Jamet, F., Vaillant, L., Tranquart, F., and Pourcelot, L. (**1999**). "High frequency (20 MHz) ultrasonic devices: Advantages and applications," Eur. J. Ultrasound **10**, 53–63.

Biwa, S., Watanabe, Y., and Ohno, N. (**2003**). "Analysis of wave attenuation in unidirectional viscoelastic composites by a differential scheme," Compos. Sci. Technol. **63**, 237–247.

Bjerknes, K., Sontum, P. C., Smistad, G., and Agerkvist, I. (**1997**). "Preparation of polymeric microbubbles: Formulation studies and product characterisation," Int. J. Pharm. **158**, 129–136.

Bossy, E., Padilla, F., Peyrin, F., and Laugier, P. (**2005**). "Three-dimensional simulation of ultrasound propagation through trabecular bone structures measured by synchrotron microtomography," Phys. Med. Biol. **50**, 5545–5556.

Bossy, E., Talmant, M., and Laugier, P. (**2004**). "Three-dimensional simulations of ultrasonic axial transmission velocity measurement on cortical bone models," J. Acoust. Soc. Am. **115**, 2314–2324.

Chaffai, S., Roberjot, V., Peyrin, F., Berger, G., and Laugier, P. (**2000**). "Frequency dependence of ultrasonic backscattering in cancellous bone: Autocorrelation model and experimental results," J. Acoust. Soc. Am. **108**, 2403–2411.

Chen, J., and Zhu, Z. (**2006**). "Ultrasound attenuation in encapsulated microbubble suspensions: The multiple scattering effects," Ultrasound Med. Biol. **32**, 961–969.

Chen, W. S., Matula, T. J., Brayman, A. A., and Crum, L. A. (**2003**). "A comparison of the fragmentation thresholds and inertial cavitation doses of different ultrasound contrast agents," J. Acoust. Soc. Am. **113**, 643–651.

Cherin, E., Brown, J., Masoy, S. E., Shariff, H., Karshafian, R., Williams, R., Burns, P. N., and Foster, F. S. (**2008**). "Radial modulation imaging of microbubble contrast agents at high frequency," Ultrasound Med. Biol. **34**, 949–962.

Cheung, K., Couture, O., Bevan, P. D., Cherin, E., Williams, R., Burns, P. N., and Foster, F. S. (**2008**). "*In vitro* characterization of the subharmonic ultrasound signal from definity microbubbles at high frequencies," Phys. Med. Biol. **53**, 1209–1223.

Chung, T. W., Tsai, Y. L., Hsieh, J. H., and Tsai, W. J. (**2006**). "Different ratios of lactide and glycolide in PLGA affect the surface property and protein delivery characteristics of the PLGA microspheres with hydrophobic additives," J. Microencapsul. **23**, 15–27.

Church, C. C. (**1995**). "The effects of an elastic solid surface layer on the radial pulsations of gas bubbles," J. Acoust. Soc. Am. **97**, 1510–1521.

Collino, F., and Tsogka, C. (**2001**). "Application of the perfectly matched absorbing layer model to the linear elastodynamic problem in anisotropic heterogeneous media," Geophysics **66**, 294–307.

Couture, O., Bevan, P. D., Cherin, E., Cheung, K., Burns, P. N., and Foster, F. S. (**2006**). "Investigating perfluorohexane particles with high-frequency ultrasound," Ultrasound Med. Biol. **32**, 73–82.

D'Astous, F. T., and Foster, F. S. (**1986**). "Frequency dependence of ultrasound attenuation and backscatter in breast tissue," Ultrasound Med. Biol. **12**, 795–808.

de Jong, N., Hoff, L., Skotland, T., and Bom, N. (**1992**). "Absorption and scatter of encapsulated gas filled microspheres: Theoretical considerations and some measurements," Ultrasonics **30**, 95–103.

Deng, C. X., Lizzi, F. L., Silverman, R. H., Ursea, R., and Coleman, D. J. (**1998**). "Imaging and spectrum analysis of contrast agents in the in vivo rabbit eye using very-high-frequency ultrasound," Ultrasound Med. Biol. **24**, 383–394.

Diaz-Lopez, R., Tsapis, N., and Fattal, E. (**2010**). "Liquid perfluorocarbons as contrast agents for ultrasonography and $^{19}$F-MRI," Pharm. Res. **27**, 1–16.

Diaz-Lopez, R., Tsapis, N., Libong, D., Chaminade, P., Connan, C., Chehimi, M. M., Berti, R., Taulier, N., Urbach, W., Nicolas, V., and Fattal, E. (**2009**). "Phospholipid decoration of microcapsules containing perfluorooctyl bromide used as ultrasound contrast agents," Biomaterials **30**, 1462–1472.

Doolittle, R. D., and Uberall, H. (**1966**). "Sound scattering by elastic cylindrical shells," J. Acoust. Soc. Am. **39**, 272–275.

Doyle, T. E. (**2006**). "Iterative simulation of elastic wave scattering in arbitrary dispersions of spherical particles," J. Acoust. Soc. Am. **119**, 2599–2610.

Eliaz, R. E., and Kost, J. (**2000**). "Characterization of a polymeric PLGA-injectable implant delivery system for the controlled release of proteins," J. Biomed. Mater. Res. **50**, 388–396.

Forsberg, F., Goldberg, B. B., Liu, J. B., Merton, D. A., Rawool, N. M., and Shi, W. T. (**1999**). "Tissue-specific US contrast agent for evaluation of hepatic and splenic parenchyma," Radiology **210**, 125–132.

Foster, F. S., Pavlin, C. J., Harasiewicz, K. A., Christopher, D. A., and Turnbull, D. H. (**2000**). "Advances in ultrasound biomicroscopy," Ultrasound Med. Biol. **26**, 1–27.

Foster, F. S., Zhang, M. Y., Zhou, Y. Q., Liu, G., Mehi, J., Cherin, E., Harasiewicz, K. A., Starkoski, B. G., Zan, L., Knapik, D. A., and Adamson, S. L. (**2002**). "A new ultrasound instrument for in vivo microimaging of mice," Ultrasound Med. Biol. **28**, 1165–1172.

Galaz, B., Haiat, G., Berti, R., Taulier, N., Amman, J. J., and Urbach, W. (**2010**). "Experimental validation of a time domain simulation of high frequency ultrasonic propagation in a suspension of rigid particles," J. Acoust. Soc. Am. **127**, 148–154.

Goertz, D. E., Frijlink, M. E., de Jong, N., and van der Steen, A. F. (**2006**). "High frequency non linear scattering from a micrometer to submicrometer sized lipid encapsulated contrast agent," Ultrasound Med. Biol. **32**, 569–577.

Goertz, D. E., Yu, J. L., Kerbel, R. S., Burns, P. N., and Foster, F. S. (**2002**). "High-frequency Doppler ultrasound monitors the effects of antivascular therapy on tumor blood flow," Cancer Res. **62**, 6371–6375.

Goldberg, D., Raichlen, J., and Forsberg, F. (**2001**). *Ultrasound Contrast Agents: Basic Principles and Clinical Applications* (Martin Dunitz, London), pp.1–440.
Goodman, R. R., and Stern, R. (**1962**). "Reflection and transmission of sound by elastic spherical shells," J. Acoust. Soc. Am. **34**, 338–344.
Haiat, G., Lhemery, A., Renaud, F., Padilla, F., Laugier, P., and Naili, S. (**2008**). "Velocity dispersion in trabecular bone: Influence of multiple scattering and of absorption," J. Acoust. Soc. Am. **124**, 4047–4058.
Haïat, G., and Naili, S. (**2011**)."Independent scattering model and velocity dispersion in trabecular bon," Biomech. Model. Mechanobiol. **10**, 95–108.
Haiat, G., Padilla, F., Barkmann, R., Dencks, S., Moser, U., Gluer, C. C., and Laugier, P. (**2005**). "Optimal prediction of bone mineral density with ultrasonic measurements in excised human femur," Calcif. Tissue Int. **77**, 186–192.
Haiat, G., Padilla, F., Cleveland, R. O., and Laugier, P. (**2006**). "Effects of frequency-dependent attenuation and velocity dispersion on in vitro ultrasound velocity measurements in intact human femur specimens," IEEE Trans. Ultrason. Ferroelectr. Freq. Control **53**, 39–51.
Haiat, G., Padilla, F., Peyrin, F., and Laugier, P. (**2007**). "Variation of ultrasonic parameters with trabecular bone properties: A three-dimensional model simulation," J. Bone Miner. Res. **12**, 1827.
Hasegawa, T., Hino, Y., Annou, A., Noda, H., Kato, M., and Inoue, N. (**1993**). "Acoustic radiation pressure acting on spherical and cylindrical shells," J. Acoust. Soc. Am. **93**, 154–161.
Hoff, L., Sontum, P. C., and Hovem, J. M. (**2000**). "Oscillations of polymeric microbubbles: Effect of the encapsulating shell," J. Acoust. Soc. Am. **107**, 2272–2280.
Hughes, M. S., Marsh, J. N., Hall, C. S., Fuhrhop, R. W., Lacy, E. K., Lanza, G. M., and Wickline, S. A. (**2005**). "Acoustic characterization in whole blood and plasma of site-targeted nanoparticle ultrasound contrast agent for molecular imaging," J. Acoust. Soc. Am. **117**, 964–972.
Insana, M. F., Wagner, R. F., Brown, D. G., and Hall, T. J. (**1990**). "Describing small-scale structure in random media using pulse-echo ultrasound," J. Acoust. Soc. Am. **87**, 179–192.
Karau, K. L., Molthen, R. C., Dhyani, A., Haworth, S. T., Hanger, C. C., Roerig, D. L., Johnson, R. H., and Dawson, C. A. (**2001**). "Pulmonary arterial morphometry from microfocal X-ray computed tomography," Am. J. Physiol. Heart Circ. Physiol. **281**, H2747–H2756.
Keller, M. W., Feinstein, S. B., and Watson, D. D. (**1987**)." Successful left ventricular opacification following peripheral venous injection of sonicated contrast agent: An experimental evaluation," Am. Heart J. **114**, 570–575.
Ketterling, J. A., Mamou, J., Allen, J. S. III, Aristizabal, O., Williamson, R. G., and Turnbull, D. H. (**2007**). "Excitation of polymer-shelled contrast agents with high-frequency ultrasound," J. Acoust. Soc. Am. **121**, EL48–EL53.
Krautkramer, J., and Krautkramer, H. (**1990**). *Ultrasonic Testing of Materials* (Springer-Verlag, New York), pp.1–677
Lanza, G. M., Wallace, K. D., Scott, M. J., Cacheris, W. P., Abendschein, D. R., Christy, D. H., Sharkey, A. M., Miller, J. G., Gaffney, P. J., and Wickline, S. A. (**1996**). "A novel site-targeted ultrasonic contrast agent with broad biomedical application," Circulation **94**, 3334–3340.
Mobley, J., Waters, K. R., Hall, C. S., Marsh, J. N., Hughes, M. S., Brandenburger, G. H., and Miller, J. G. (**1999**). "Measurements and predictions of the phase velocity and attenuation coefficient in suspensions of elastic microspheres," J. Acoust. Soc. Am. **106**, 652–659.
Moran, C. M., Ross, J. A., Cunningham, C., Butler, M., Anderson, T., Newby, D., Fox, K. A., and McDicken, W. N. (**2006**). "Manufacture and acoustical characterisation of a high-frequency contrast agent for targeting applications," Ultrasound Med. Biol. **32**, 421–428.
O'Donnell, M., and Miller, J. G. (**1981**). "Quantitative broadband ultrasonic backscatter: An approach to nondestructive evaluation in acoustically inhomogeneous materials," J. Appl. Phys. **52**, 1056–1065.
Pisani, E., Tsapis, N., Galaz, B., Santin, M., Berti, R., Taulier, N., Kurtisovski, E., Lucidarme, O., Ourevitch, M., Doan, B. T., Beloeil, J. C., Gillet, B., Urbach, W., Bridal, S. L., and Fattal, E. (**2008**). "Perfluorooctyl bromide polymeric capsules as dual contrast agents for ultrasonography and magnetic resonance imaging," Adv. Funct. Mater. **18**, 2963–2971.
Pisani, E., Tsapis, N., Paris, J., Nicolas, V., Cattel, L., and Fattal, E. (**2006**). "Polymeric nano/microcapsules of liquid perfluorocarbons for ultrasonic imaging: Physical characterization," Langmuir **22**, 4397–4402.
Postema, M., and Schmitz, G. (**2007**). "Ultrasonic bubbles in medicine: Influence of the shell," Ultrason. Sonochem. **14**, 438–444.
Powers, J. M., and Caddell, R. M. (**1972**). "The macroscopic volume changes of selected polymers subjected to uniform tensile deformation," Polym. Eng. Sci. **12**, 432–436.
Rapoport, N., Gao, Z., and Kennedy, A. (**2007**). "Multifunctional nanoparticles for combining ultrasonic tumor imaging and targeted chemotherapy," J. Natl. Cancer Inst. **99**, 1095–1106.
Roberjot, V., Laugier, P., Droin, P., Giat, P., and Berger, G. (**1996**). "Measurement of integrated backscatter coefficient of trabecular bone," in *Proceedings of the IEEE Ultrasonics Symposium*, pp.1123–1125.
Sarkar, K., Shi, W. T., Chatterjee, D., and Forsberg, F. (**2005**). "Characterization of ultrasound contrast microbubbles using *in vitro* experiments and viscous and viscoelastic interface models for encapsulation," J. Acoust. Soc. Am. **118**, 539–550.
Schneider, M. (**1999**). "Characteristic of SonoVue," Echocardiogr. **16**, 743–746.
Stride, E., and Saffari, N. (**2005**). "Investigating the significance of multiple scattering in ultrasound contrast agent particle populations," IEEE Trans. Ultrason. Ferroelectr. Freq. Control **52**, 2332–2345.
Sun, Y., Kruse, D. E., Dayton, P. A., and Ferrara, K. W. (**2005**). "High-frequency dynamics of ultrasound contrast agents," IEEE Trans. Ultrason. Ferroelectr. Freq. Control **52**, 1981–1991.
Ugincius, P., and Uberall, H. (**1968**). "Creeping-wave analysis of acoustic scattering by elastic cylindrical shells," J. Acoust. Soc. Am. **43**, 1025–1035.
Waterman, P. C., and Truell, R. (**1961**). "Multiple-scattering of waves," J. Math. Phys. **2**, 512–537.
Yang, R. B., and Mal, A. K. (**1994**). "Multiple-scattering of elastic waves in a fiber-reinforced composite," J. Mech. Phys. Solids **42**, 1945–1968.